BIOCHEMISTRY
including biophysical chemistry & molecular biology

Article

pubs.acs.org/biochemistry

Structure-Based Engineering of a Minimal Porin Reveals Loop-Independent Channel Closure

Wolfgang Grosse,[†,‡] Georgios Psakis,[†,§] Barbara Mertins,[†] Philipp Reiss,[†] Dirk Windisch,[∥] Felix Brademann,[†] Jochen Bürck,[∥] Anne Ulrich,[∥] Ulrich Koert,[†] and Lars-Oliver Essen*[,†]

[†]Department of Chemistry, Philipps-University Marburg, Hans-Meerwein-Straße, 35032 Marburg, Germany

[‡]SB-ISIC-LCPPM, Ecole Polytechnique Fédérale de Lausanne, Station 6, 1015 Lausanne, Switzerland

[§]Chemical and Biological Sciences, University of Huddersfield, Queensgate, Huddersfield HD1 3DH, Great Britain

[∥]Institute for Biological Interfaces (IBG2) and Institute of Organic Chemistry (IOC), Karlsruhe Institute of Technology (KIT), Fritz-Haber-Weg 6, 761311 Karlsruhe, Germany

Supporting Information

ABSTRACT: Porins, like outer membrane protein G (OmpG) of *Escherichia coli*, are ideal templates among ion channels for protein and chemical engineering because of their robustness and simple architecture. OmpG shows fast transitions between open and closed states, which were attributed to loop 6 (L6). As flickering limits single-channel-based applications, we pruned L6 by either 8 or 12 amino acids. While the open probabilities of both L6 variants resemble that of native OmpG, their gating frequencies were reduced by 63 and 81%, respectively. Using the 3.2 Å structure of the shorter L6 variant in the open state, we engineered a minimal porin (220 amino acids), where all remaining extramembranous loops were truncated. Unexpectedly, this minimized porin still exhibited gating, but it was 5-fold less frequent than in OmpG. The residual gating of the minimal pore is hence independent of L6 rearrangements and involves narrowing of the ion conductance pathway most probably driven by global stretching−flexing deformations of the membrane-embedded β-barrel.

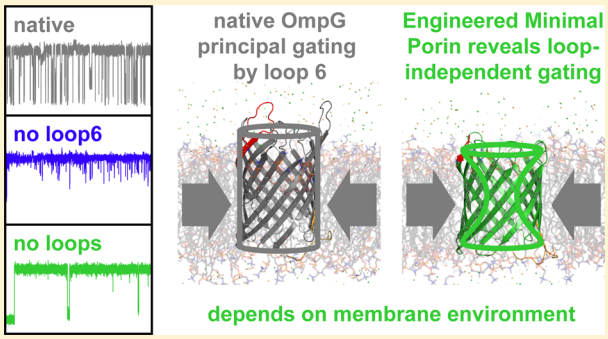

Ion channel engineering aims to alter the electrophysiological properties of biological pores and/or channels and to potentially change them into tunable molecular switches, e.g., for the design of new biological tools[1−5] or to develop them into alternative therapeutics.[1,6−8] For rational engineering and applications like stochastic sensing, the starting template is crucial. Porins, like trimeric outer membrane protein F (OmpF) from *Escherichia coli*[9−11] or the heptameric single-barrel porin from *Staphylococcus aureus* α-hemolysin (αHL),[4,12−14] have been subjected to extensive engineering, but their multimeric nature hampers fine modulation of their pore regions. OmpG from *E. coli*, however, has recently attracted significant attention because of its monomeric nature and the ease with which it can be modified. For engineering, OmpG is a promising template, because it forms a robust 14-stranded β-barrel with a wide, nonselective pore, which exhibits voltage- and pH-dependent gating caused by loop-driven transitions.[15−19] Current strategies for OmpG aim to deconstruct the pore or narrow the lumen permeability by introducing modulators at single or double attachment sites[20] to transform it into a more ion- or substrate-specific porin.

Extracellular loops of outer membrane proteins exhibit a vast repertoire of functions, ranging from the enhancement of cellular integrity[21] and control of substrate permeation[22] to mediation of pathogen−host interactions[23] and increasing bacterial virulence.[24] Crystal structures of OmpG at neutral [Protein Data Bank (PDB) entry 2IWV; pH 7.5] and acidic (PDB entry 2IWW; pH 5.6) pH have revealed considerable differences in the conformations of its extracellular loops.[19] L6, connecting strands β11 and β12, underwent the largest rearrangements by folding from an extended conformation at neutral pH into the OmpG cavity at acidic pH and thus occluding the pore (Figure 1A). Differences in the H-bonding networks in the two structures allowed the identification of a histidine pair (H231/H261), whose protonation states apparently determine the formation or breakage of these networks and potentially act as a pH switch controlling the open versus closed state of the pore.[19] OmpG in planar lipid bilayers undergoes pH-dependent rapid fluctuations between the two states manifesting themselves as intense "noise" in current recordings.[25] Consequently, for the development of OmpG into a template useful for protein engineering, initial strategies focused on the elimination of this intrinsic noise. Immobilization of L6 by the introduction of disulfide bonds at

Received: May 29, 2014
Revised: July 1, 2014
Published: July 2, 2014

   dx.doi.org/10.1021/bi500660q | *Biochemistry* 2014, 53, 4826−4838

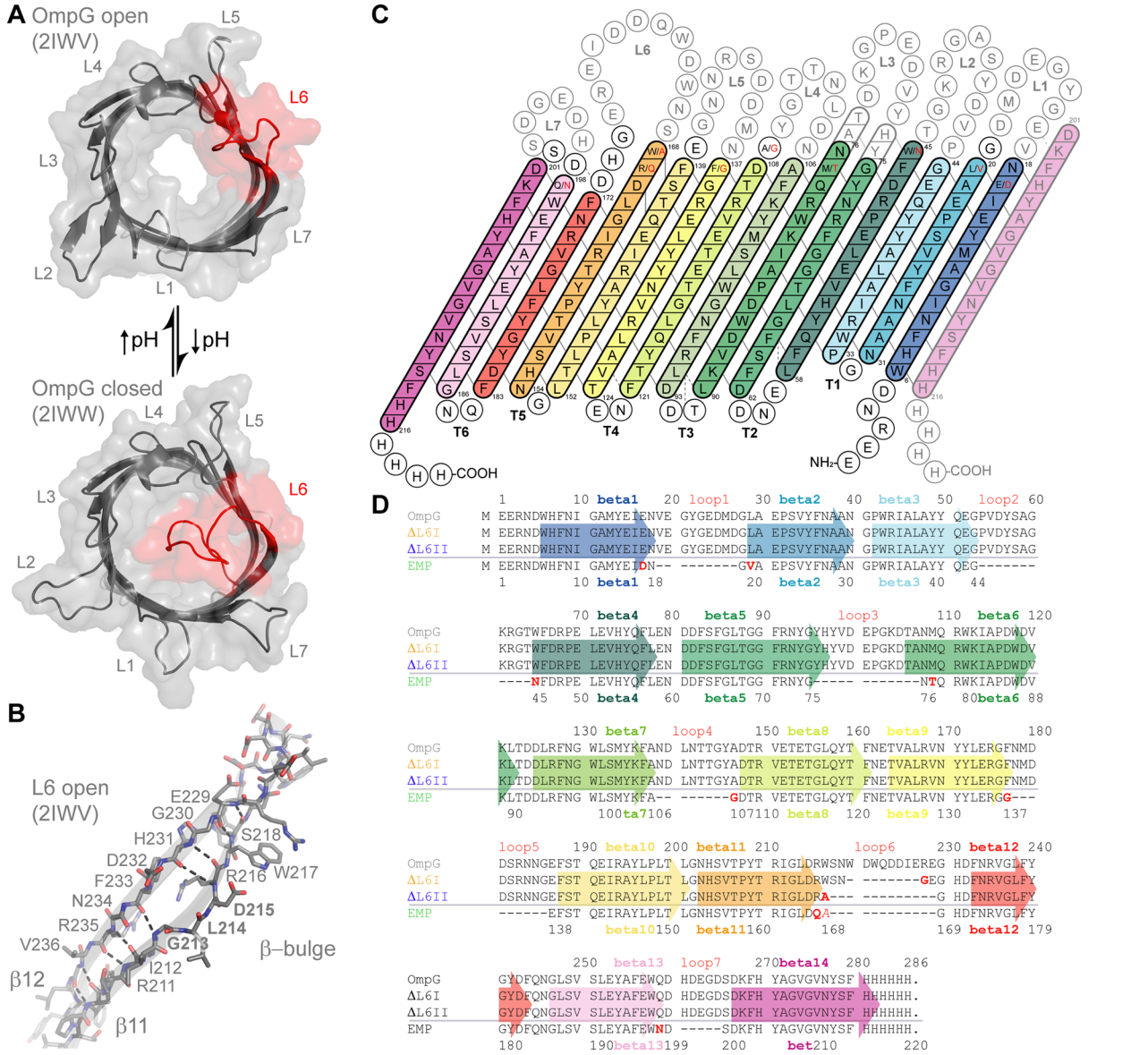

Figure 1. OmpG, L6-mediated gating and EMP design. (A) Surface representations of the open (PDB entry 2IWV) and closed (PDB entry 2IWW) OmpG structures, viewed from the top. At acidic pH, H231 (β12) and H261 (L7) are protonated, their repulsion causing L6 to extend toward the hydrophilic cavity closing the channel. (B) Side view of the β11–L6–β12 hairpin in the 2IWV structure. (C) Topology of OmpG (opaque) with rainbow-colored transmembrane β-strands. Strand β14 is repeated on the N-terminal side, reflecting the β-barrel assembly. Gray lines between strands indicate the H-bonding network; the topology of EMP is colored black, and introduced mutations are colored red. (D) Sequence alignment of OmpG and its variants, in which strands are colored using the same scheme used in panel C.

the extracellular side of strands β12 and β13, as well as optimization of the H-bonding network between strands β11 and β12 by removal of a β-bulge (Figure 1B) in strand β11 (ΔD215), considerably reduced the extent of rapid switching.[15] However, infrequent closure of the channel still occurred. Later work[26] implied that as long as the H231/H261 pair is present, OmpG variants (like OmpGΔL6) are still capable of responding to pH changes, thus explaining the rare closing events observed previously.[15] The crystal structure of the $OmpG_{ALA}$ variant (H231A/H261A; PDB entry 2X9K), however, still shared features of both the open and closed states of OmpG, with L6 and L7 acquiring a somewhat intermediate conformation between the two states. Interestingly, Fourier transform infrared (FTIR) spectroscopy studies of this mutant suggested a lock in the open state,[26] but this behavior was not confirmed by conductance analyses. Investigations by paramagnetic relaxation enhancement nuclear magnetic resonance (NMR) could verify fast, pH-dependent movements of L6.[27] Two of three main ensembles observed, in the latter study, resembled the crystal structures of the open and closed conformations, while strong influences on gating were observed in cysteine-based cross-linking experiments.

For engineering an improved template, we pruned OmpG first at its L6 by 8 (ΔL6I; OmpG/Δ220–227/R228G) and 12 (ΔL6II; OmpG/Δ218–229/W217A) amino acids, while leaving the H231/H261 pair and the β-bulge intact, and determined the resulting structure at 3.2 Å resolution. We further designed an engineered minimal porin (EMP) by shortening all extramembranous OmpG loops to simple β-turns (Figure 1C) and investigated its gating characteristics.

dx.doi.org/10.1021/bi500660q | Biochemistry 2014, 53, 4826–4838

Table 1. CD and OCD Parameters of OmpG-like Porins in Vesicles and Micelles

	CD						
	20 °C, native			20 °C, heat-denatured			
in LDAO	λ_{MAX} (nm)	λ_{MIN} (nm)	MRE_{MAX}:MRE_{MIN} ratio[a]	λ_{MAX} (nm)	λ_{MIN} (nm)	MRE_{MAX}:MRE_{MIN} ratio[a]	$ratio_{native}$:$ratio_{denat.}$
OmpG	192.0	217.5	2.3	192.0	218.0	1.6	1.4
ΔL6I	196.5	217.0	2.6	192.5	216.5	1.9	1.4
ΔL6II	195.0	214.5	3.3	190.0	216.0	2.3	1.4
EMP	192.5	215.5	1.9	191.0	212.5	0.8	2.4
	CD						
	20 °C			35 °C			
in DMPC	λ_{MAX} (nm)	λ_{MIN} (nm)	MRE_{MAX}:MRE_{MIN} ratio	λ_{MAX} (nm)	λ_{MIN} (nm)	MRE_{MAX}:MRE_{MIN} ratio	$ratio_{20\ °C}$:$ratio_{35\ °C}$
OmpG	196.0	218.3	1.9	195.0	216.5	1.7	1.1
ΔL6I	192.5	216.2	2.8	192.7	216.1	2.6	1.1
ΔL6II	196.5	218.0	2.6	195.0	216.5	2.0	1.3
EMP	193.3	219.3	4.2	192.4	217.2	2.9	1.4
	OCD						
	20 °C			35 °C			
in DMPC	λ_{MAX} (nm)	λ_{MIN} (nm)	OCD_{MAX}:OCD_{MIN} ratio	λ_{MAX} (nm)	λ_{MIN} (nm)	OCD_{MAX}:OCD_{MIN} ratio	$ratio_{20\ °C}$:$ratio_{35\ °C}$
OmpG	198.2	218.9	7.3	191.8	221.4	6.1	0.9
ΔL6I	196.0	218.5	2.2	191.2	218.5	2.4	0.9
ΔL6II	196.5	214.1	2.2	–	–	–	–
EMP	188.8	220.4	6.9	188.8	217.4	2.0	3.5

[a]Note that MRE_{MAX}:MRE_{MIN} ratios for measurements using LDAO micelles are less reliable than for DMPC, as the intense noise in the 190−200 nm part of the spectrum prevented the exact identification of maxima. The increased noise was also indicated by an increase in the magnitude of the HT voltage signal.

MATERIALS AND METHODS

Extended and more detailed descriptions of all methods can be found in the Supporting Information under Supporting Experimental Procedures 3.1−3.9.

Construct Design, Mutagenesis, and Protein Production. The gene encoding OmpG (residues 22−301; UniProt entry P76045) with a C-terminal His tag was cloned in the pET20b(+) vector as described previously.[20] L6 deletion variants OmpG/Δ220−227/R228G (ΔL6I) and OmpG/Δ218−229/W217A (ΔL6II) were produced from this plasmid, while the EMP sequence (220 amino acids) was synthesized (Geneart, Invitrogen Life Technologies) (Figure 1). Recombinant OmpG variants were produced as inclusion bodies in porin-deficient *E. coli*[28] and *a priori* purified by being washed, as previously described[20] (sections 3.1 and 3.2 of the Supporting Information).

Spontaneous Refolding of Denatured Proteins. For refolding into unilamellar lipid vesicles, OmpG and its variants were dissolved in 6 M urea buffer and diluted 10-fold into vesicle-containing buffer. Vesicles were preformed from 1,2-dimyristoyl-*sn*-glycero-3-phosphocholine (DMPC), 1,2-dioleoyl-*sn*-glycero-3-phosphocholine (DOPC), or 1,2-dipalmitoyl-*sn*-glycero-3-phosphocholine (DPPC) (Avanti Polar Lipids).[29,30]

For refolding in detergent, OmpG and the L6 truncations were dissolved in 6 M urea buffer and rapidly diluted in *n*-octyl β-D-glucopyranoside (OG)-containing buffer, and unfolded protein was removed by proteinase K treatment.[25] EMP was dissolved in 6 M guanidinium chloride buffer and dialyzed in two steps in the presence of lauryl-dimethylamine-*N*-oxide (LDAO)-containing buffer[31] (section 3.3 of the Supporting Information).

Protein Purification. Refolded OmpG, ΔL6I, and ΔL6II were purified in the presence of *n*-octyl tetraoxyethylene (C_8E_4) using a HiTrap DEAE Sepharose anion exchange column (GE Healthcare), while EMP was purified in the presence of LDAO with a TALON metal affinity column (GE Healthcare). SEC was performed with Superdex200 resin (GE Healthcare) (section 3.4 of the Supporting Information).

Reconstitution into Lipid Vesicles for CD and OCD Studies. Proteins refolded in detergent micelles were reconstituted in preformed liposomes as described in section 3.5 of the Supporting Information. Detergent−lipid exchange was mediated by the adsorption of the detergent to biobeads (Bio-Rad). Nonreconstituted forms of OmpG were removed by centrifugation and ultrafiltration. The lipid content was monitored by thin-layer chromatography (TLC)[29,32,33] (Figure S8 of the Supporting Information).

CD and OCD Measurements. CD studies were performed using a J-810 or J-815 spectropolarimeter (Jasco).[34,35] Spectra in LDAO micelles were recorded at 20 °C and spectra in DMPC at 20 and 35 °C. Thermal denaturation was monitored at the corresponding CD minima (Table 1), and the temperature was varied from 10 to 95 °C. Spectra were recorded at 20 °C before and after the temperature ramps. Secondary structure predictions were performed using the CONTIN-LL algorithm[36,37] of the DICHROWEB server.[38−40]

For OCD studies, the lipoprotein sample was deposited on a quartz glass plate and dried at room temperature under a gentle stream of air. Samples were subsequently hydrated at the desired temperature for 15 h in the OCD cell (relative humidity of 97−99%)[35,41] (section 3.6 of the Supporting Information).

Single-Channel Recordings in Planar Lipid Bilayers. Porin conductances were electrophysiologically monitored in 1,2-diphytanoyl-*sn*-glycero-3-phosphocholine (DPhPC) (Avanti Polar Lipids) and asolectin (Avanti Polar Lipids). Membranes were generated by painting in a two-chamber apparatus; detergent-refolded and -purified porins were added to one compartment next to the planar lipid bilayer, and a voltage

dx.doi.org/10.1021/bi500660q | Biochemistry 2014, 53, 4826−4838

gradient was imposed while waiting for the insertion of single channels.[20]

Open probability P_o is the time the porin lingers in fully or partly open states divided by the total recording time. States exhibiting a >80% reduction in their current were considered to be fully closed. The frequency of open to closed/partly closed transitions (f) was expressed as the number of observed events per unit of time (number of events per second). P_o and f values represent the average of triplicate measurements (±SEM) (section 3.7 of the Supporting Information).

Crystallization and Determination of the Structure of ΔL6II. Crystallization of ΔL6II was performed using commercial screens as well as optimized buffer conditions[18] in 24- and 96-well sitting-drop plates. Diffraction data of the ΔL6II variant were collected at ID 14-1 at the ESRF (Grenoble, France) at 3.2 Å resolution (100 K). Data were indexed and integrated in space group $P1$ using XDS and scaled with Scala (Table 2).[42] The structure was determined using AutoMR,[43]

Table 2. Crystallographic Data of the ΔL6II Variant (PDB entry 4CTD)

Data Collection and Processing	
X-ray source	ID 14-1, ESRF
wavelength (Å)	0.9334
detector	ADSC Quantum Q210
temperature (K)	100
space group	$P1$
no. of molecules per asymmetric unit	2
cell dimensions	
a, b, c (Å)	59.9, 60.1, 59.8
α, β, γ (deg)	70.5, 95.2, 70.6
resolution (Å)[a]	44.2−3.2 (3.37−3.20)
no. of reflections	19941
no. of unique reflections	11053
multiplicity[a]	1.8 (1.8)
R_{merge}[a,b]	0.152 (0.539)
completeness (%)[a]	92.8 (93.9)
$\langle I\rangle/\sigma\langle I\rangle$[a]	5.3 (2.0)
mosaicity (deg)	0.798
Wilson B factor (Å^2)	35.1
water content	0.579
Refinement	
resolution (Å)[a]	44.21−3.2 (3.522−3.200)
R_{work}, R_{free} (%)[a,c,d]	23.8, 28.9 (25.3, 29.8)
no. of reflections (work, test set)[a,d]	10858, 529
rmsd from ideal for bonds (Å)	0.015
rmsd from ideal for angles (deg)	1.311
no. of atoms (total; protein, hetero, waters)	3848; 3774, 74, 0
mean B factor (total; protein, hetero) (Å^2)[e]	17.8 (50.1); 50.2, 48.0

[a]Values in parentheses correspond to those of the highest-resolution shell. [b]$R_{merge} = \sum_{hkl}\sum_i|I_i(hkl) - \langle I(hkl)\rangle|/\sum_{hkl}\sum_i I_i(hkl)$. [c]$R_{work} = \sum|F_{obs} - F_{calc}|/\sum(F_{obs})$. [d]$R_{free}$ is the crystallographic R factor based on 4.9% of the data not used in refinement. [e]The value in parentheses corresponds to the mean B factor without TLS refinement.

and structure factors were anisotropy-corrected. Coot[44] was used for manual model building, and the structure was refined with PHENIX,[45] yielding final R_{work} and R_{free} values of 0.238 and 0.289, respectively [0.253 and 0.298, respectively, in highest-resolution shell (Table 2), PDB entry 4CTD]. Crystal contacts in the packing were analyzed with the PISA server[46] (section 3.8 of the Supporting Information).

Molecular Dynamics Simulations. Homology models of OmpG and OmpG variants were generated with Modeler version 9.10,[47,48] and protonation states of the side chains were determined using the H++ server.[49−52] The systems were built and assembled in a DMPC membrane using the CHARMM-GUI Membrane Builder,[53,54] equilibrated by NAMD-2.8 and general CHARMM force field 2b7[55] using an *NPT* ensemble with periodic boundary conditions. The equilibrated systems were used in a 40 ns run. Electrostatic surface potentials were calculated using the PyMol APBS tool[56] (section 3.9 of the Supporting Information).

RESULTS

Denatured L6 Deletion Variants Spontaneously Refold into Lipids Different from Those of OmpG. Successful membrane insertion of unfolded OmpG and its variants into preformed DMPC, DOPC, or DPPC unilamellar vesicles was confirmed by analyzing unheated and boiled sodium dodecyl sulfate−polyacrylamide gel electrophoresis (SDS−PAGE) samples. Misfolded OmpG migrated more slowly (~36 kDa) during SDS−PAGE than the folded membrane-inserted counterparts (~29 kDa) (Figure S1 of the Supporting Information). OmpG exhibited preferential insertion into DPPC (16:0 PC) vesicles, whereas both L6 deletion variants reconstituted only into DMPC (14:0 PC) vesicles. Furthermore, none of the urea-denatured OmpG-derived porins incorporated into DOPC vesicles [18:1 (Δ9-cis) PC] (Figure S1 of the Supporting Information). Consequently, porin refolding and reconstitution in lipid vesicles, in the absence of detergent, appeared to be L6-dependent, as shorter L6 loop variants required phospholipids with shorter acyl chains. Densitometric analysis of the gels showed that refolding yields were limited to 20−30% for direct insertion into lipid bilayers and not affected by the lipid:protein molar ratios [100:1−300:1 (Figure S1 of the Supporting Information)]. For comparison, detergent-refolded OmpG variants subsequently reconstituted into vesicles or artificial bilayers achieved insertion efficiencies of 40 to >70%.

The structural integrity of the refolded monomeric OmpG variants was assessed by circular dichroism (CD). All analyzed variants displayed typical β-barrel line shapes (Figure S2 of the Supporting Information and Table 1). Thermal denaturation of OmpG, ΔL6I, and ΔL6II in LDAO detergent micelles showed cooperative unfolding as indicated by sigmoidal melting curves with an apparent melting temperature of 77 °C (Figure S2 of the Supporting Information). Upon cooling to 20 °C, OmpG and the L6 deletion variants showed a hypsochromic shift of the 215 nm band and a reduction of the CD bands, thus indicating incomplete refolding. For qualitative comparisons, we considered the maximum:minimum ellipticity ratios before and after thermal denaturation and refolding. Changes in these ratios reflect overall changes in the integrity of the secondary structure (Table 1). For OmpG, the ratio was reduced from 2.3 to 1.6 (~30%); comparable changes were found for the L6 deletion variants. Overall, when denatured OmpG variants were cooled, their β-sheet and turn content increased without reaching nativelike values.

Structural Integrity of L6 Deletion Variants in DMPC Bilayers. For secondary structure predictions, as well as for oriented CD (OCD) measurements, detergent-refolded OmpG variants were reconstituted in DMPC vesicles, because these mimic the natural membranes better than micelles and the chosen procedure guarantees a high degree of purity for

dx.doi.org/10.1021/bi500660q | Biochemistry 2014, 53, 4826−4838

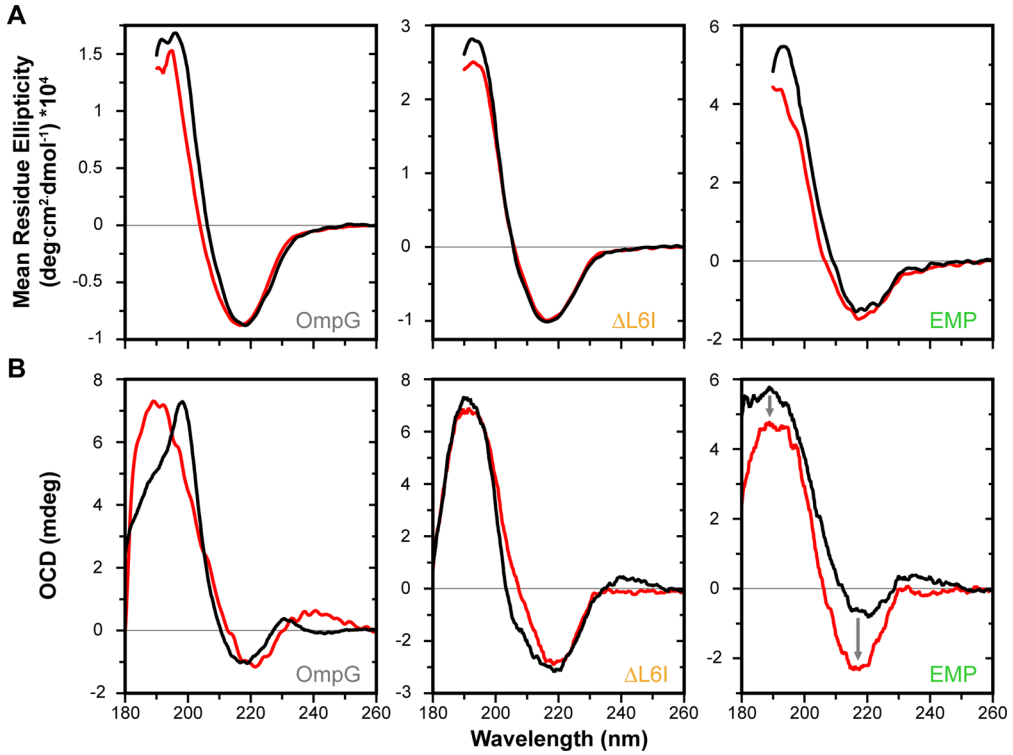

Figure 2. CD and OCD spectra of OmpG, the ΔL6I variant, and EMP in DMPC. Spectra were recorded below (20 °C, black) and above (35 °C, red) the DMPC-phase transition temperature. (A) Far-UV spectra and (B) OCD spectra. Gray arrows indicate directional changes in the EMP spectra. The ratio of the positive and negative OCD signals indicates the tensor of the β-barrel.

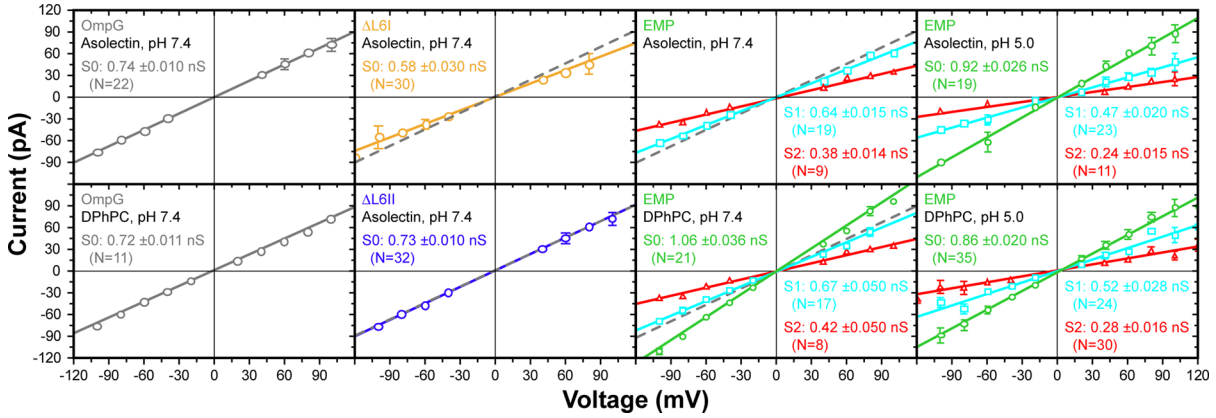

Figure 3. Ohm plots for conductances of OmpG and its variants. OmpG conducts similarly in asolectin and DPhPC at pH 7.4 (gray lines). The conductance of ΔL6I in asolectin at pH 7.4 (yellow line) is reduced; ΔL6II (blue line) conducts as strongly as native OmpG. The EMP conductance varies with the pH and type of lipid. In asolectin and at neutral pH, EMP occupies only partially closed states (cyan for S_1 and red for S_2), and at acidic pH, it additionally acquires a fully open state (green for S_0). In DPhPC, the behavior of EMP is inverted as it conducts more strongly at neutral rather than acidic pH. The OmpG conductance appears in all graphs as a dashed gray line.

incorporated OmpG porins. CD spectra were recorded below and above the lipid-phase transition temperature to investigate the influence of the bilayer phase on reconstitution and secondary structure. In general, the CD spectra resembled those obtained for OmpG in detergent micelles, confirming that the native OmpG and the L6 deletion variants are well-folded in lipid bilayers (Figure 2 and Figure S2 of the Supporting Information). Secondary structure predictions by deconvolution of the CD spectra showed contents of ∼47% β-strand, ∼8% α-helix, ∼9% β-turn, and ∼36% unstructured parts for OmpG, which deviated only mildly from the values for previously published OmpG structures (Table S1 of the Supporting Information). For the L6 deletion variants, similar contents were found.

For deciphering the membrane orientation of β-sheet proteins by OCD, quantitative theory and evaluation procedures are still missing. However, the intensities of positive (∼195 nm) and negative (∼215 nm) bands provide an indication of the preferred orientation of β-sheet proteins relative to the membrane.[57] The presence of the negative band and the intensity ratio of the positive band to the negative band can be used in combination with reference spectra as an indication to estimate the orientation of β-strand proteins (Supporting Information). Compared to the CD spectrum of

dx.doi.org/10.1021/bi500660q | Biochemistry 2014, 53, 4826−4838

isotropic vesicle samples, the OCD spectrum of OmpG in macroscopically aligned DMPC bilayers showed at both 20 and 35 °C a much stronger positive amplitude (190 nm), while the negative amplitude (~222 nm) remained almost identical (Figure 2), indicating a preferential orientation in the bilayer. The calculated intensity ratio of 7.3 for oriented OmpG (OmpG in isotropic vesicles, 1.9) reflects a linear combination of the two reference spectra for β-strands that are aligned either parallel (slightly more strongly represented in the case of OmpG) or perpendicular to the membrane normal. For comparison, the shear number of 18 for OmpG implies a barrel tilt of 43° relative to the membrane plane.[18] The OCD spectra of the ΔL6I variant in DMPC at 20 and 35 °C were similar (Figure 2), thus demonstrating that its orientation within the membrane is unaffected by the L6 truncation.

L6 Dominates Spontaneous Gating of OmpG but Does Not Control Full Closure. The conductance and gating behavior of OmpG and its variants were derived by BLM experiments in asolectin and DPhPC membranes. Compared to that of OmpG (with asolectin, 0.74 ± 0.010 nS and N = 22; with DPhPC, 0.72 ± 0.011 nS and N = 11), the ΔL6I-dependent conductance (Figure 3) in asolectin (pH 7.4) was ~1.3-fold lower (0.58 ± 0.030 nS, N = 30, and $P < 10^{-3}$). We attribute this reduction to infrequent switching events, which caused partial closure of the pore (Figure S3 of the Supporting Information). Further shortening of L6 as given by the ΔL6II variant restored wild-type-like conductance (0.73 ± 0.010 nS, and N = 32). Apparently, the WSNGE motif in L6 in the ΔL6I variant that is absent in the ΔL6II variant (Figure 1C) suffices to support a partly closed state of OmpG. Although the electrophysiological data originated from several protein batches, the porins' gating and conductances were found to be batch-independent.

As expected, the successively shortened L6 loops of the OmpG variants progressively reduced the rapid open-to-closed state transitions (gating frequency f) with respect to native OmpG, as indicated by the lower occurrence of the long downward current spikes in the 80 mV traces (Figure 4A). Intact OmpG remained fully open (≥90% of I_o) or partly closed (≤20% of I_o), showing events with dwell times between 10 μs and 316 ms. Both ΔL6I and ΔL6II displayed distributions of conductances similar to that of intact OmpG, but their dwell times of events were increased up to 100 and 5 s, respectively (Figure 4B). The increases in the mean dwell times, for both deletion variants, coincided with a decrease in the level of spontaneous gating. ΔL6I exhibited an ~3-fold decrease and ΔL6II an ~5-fold decrease in their spontaneous transition frequencies, f (Figure 4C), while sharing with OmpG the same global probability for occupying an open state (P_o). However, complete closure events in the L6 deletion variants still occurred, as indicated by the infrequent but prominent current spikes, despite the fact that the putatively principal element responsible for gating was removed.

Crystal Structure of the ΔL6II OmpG Variant in the Open State. To analyze structural changes caused by the L6 truncations, we crystallized the ΔL6II variant and determined its structure in space group $P1$ at 3.2 Å resolution (Table 2). Anisotropy-corrected electron density maps showed two well-defined β-barrels of ΔL6II in the asymmetric symmetry unit (asu), including the short periplasmatic turns and less defined extracellular loop regions (Figure 5A). Several strong density features close to charged residues were assigned as chloride ions. Difference density maps further revealed long tubular

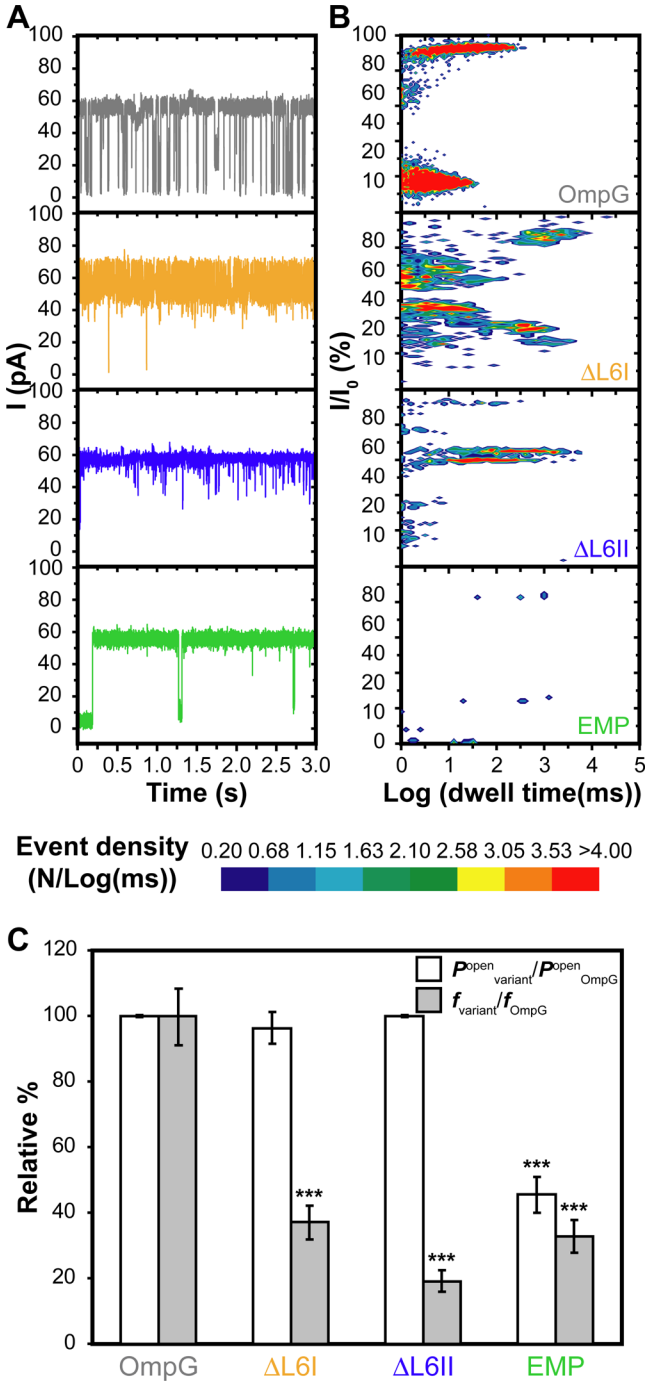

Figure 4. Gating characteristics of OmpG and OmpG variants. (A) Typical 80 mV single-channel recordings at pH 7.4 in asolectin used for the generation of the 2D event distribution plots in panel B. (B) 2D event distribution plots of the switching behavior. The distribution of events for 30 s of recorded time is plotted according to current intensity I and dwell times. I is expressed as a percentage of the highest intensity I_o. The density of events is color-coded as indicated below the graphs. (C) Comparison of the gating behavior of OmpG and OmpG variants (Table S2 of the Supporting Information). f and P_o are expressed as a percentage of the OmpG parameters. Bars denote standard errors of triplicate measurements and asterisks statistically significant differences (paired t test with $P \leq 0.0050$) with respect to the corresponding OmpG values.

structures close to crystal contacts that were modeled as two complete and two partly defined C_8E_4 molecules (Figure 5A).

dx.doi.org/10.1021/bi500660q | Biochemistry 2014, 53, 4826−4838

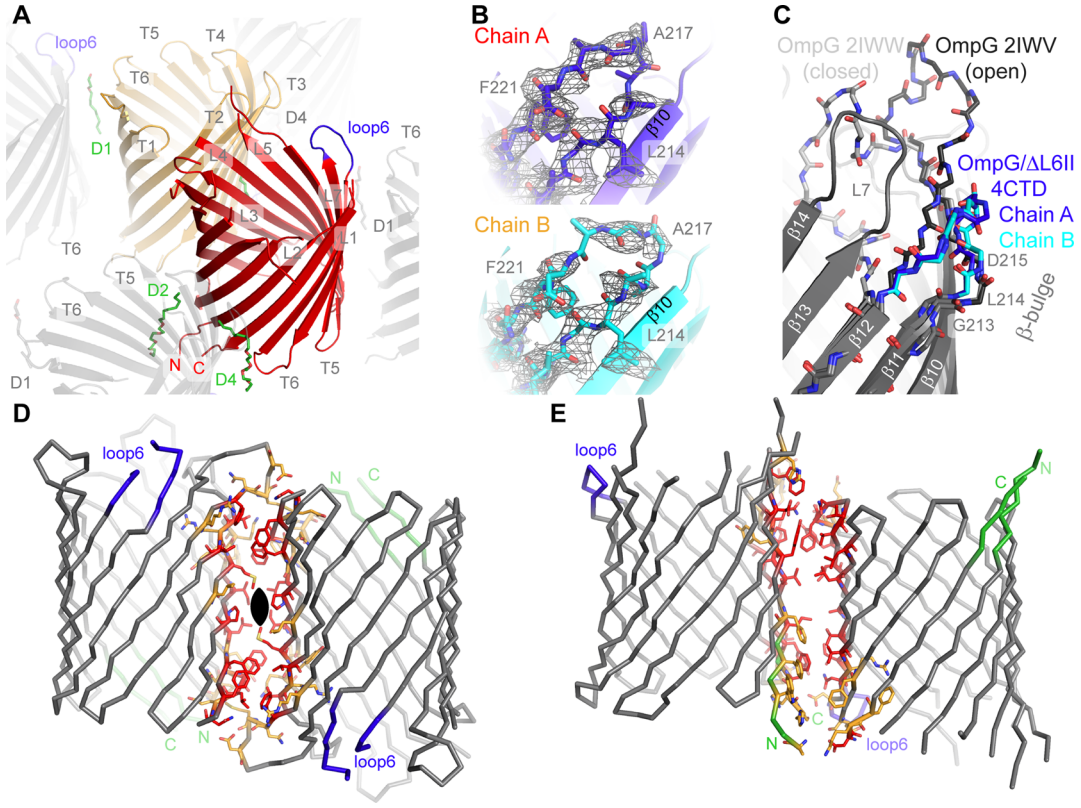

Figure 5. Crystal structure of ΔL6II and crystallization interfaces. (A) View of the pore (red for chain A, yellow for chain B, and gray for symmetry equivalent molecules) in the plane of the crystal lattice, including the shortened L6 (blue) and the modeled C_8E_4 molecules (green). (B) SIGMAA-weighted OMIT electron densities calculated for L6 at 3.2 Å. L6 exhibits two different conformations, in the defined $F_{obs} - F_{calc}$ (contouring level of $1.0\sigma \equiv 0.33$ e/Å^3) OMIT densities. (C) Superposition of the 2IWW (closed), 2IWV (open), and ΔL6II crystal structures. (D and E) At least one interface is represented in each deposited crystal structure: C2 symmetric interface I (D) or antiparallel, nonsymmetric interface II (E). Amino acids identified as interaction partners in all (some) reported interfaces are colored red (yellow).

Within the hydrophobic plane, each β-barrel contacts one NCS- and two symmetry-related porins in an antiparallel fashion, yielding the fifth distinct crystal packing of OmpG (Figure S4 of the Supporting Information). This crystal form, as well as those of PDB entries 2F1C[18] and 2WVP,[20] depends on type I interactions, in which alternating barrels bury major parts of their hydrophobic surfaces in contact regions (Results of the Supporting Information and Figure 5D,E). Additionally, the detergent molecules occupied positions different from those occupied in the two previous OmpG crystal structures determined previously in space group C2 (2F1C and 2WVP).

The ΔL6II porin structure closely resembled all previous OmpG structures with Cα displacements for the β-barrel being $\ll$1 Å. The backbone of the shortened L6, as observed in both ΔL6II molecules, revealed two slightly different conformations, both leaving the ΔL6's ion conducting tunnel unaffected (Figure 5B). Furthermore, the trace of L6 shortened to a β-hairpin left the preceding β-bulge (G213-L214-D215) intact (Figure 5C). Compared to the two previous structures of OmpG in space group C2, different conformations were observed for the L2 and L5 loops, probably stemming from (a) a lack of L6-driven stabilizing interactions or (b) differences in crystal packing.

Modeling and MD Simulations of EMP. The design of the minimal porin was based on the H-bonding network of the available crystal structures and was modeled on chain A of the open state OmpG (PDB entry 2IWV)[19] because of its well-resolved loop regions (Figure S5 of the Supporting Information). As the structural models were based on crystallographic data, fast equilibration times were achieved. In the 40 ns simulations, the rmsd for the non-H protein atoms increased within ~17 ns to a plateau and remained constant for the remainder of the simulation. No unfolding events were observed in the EMP simulations. It is noteworthy that for the OmpG and ΔL6II barrel, certain portions protruded above the membrane, while the shorter engineered minimal pore was almost completely buried (Figure 6A). In all simulations, the β-barrel was almost invariant unlike the flexible loop regions. The relative mobility (B factor) was calculated over the last 20 ns (stable rmsd for the protein) (Figure S6 of the Supporting Information) and resembled those of NMR and X-ray studies.[27] Electrostatic surface calculations revealed a reduction in the electrostatic potential of ΔL6II and an almost complete lack of overall charge for EMP, resulting from the reduction of the negative charges in the loops (Figure 6B). This observation correlates with the variable behavior of the porin templates in different lipidic environments.

Biochemical and Biophysical Characteristics of the EMP Channel. The folding of the engineered minimal porin that has a surface charge significantly reduced compared to that of OmpG could not be monitored by SDS−PAGE analyses, because folded and unfolded species displayed identical migration behavior (Figure S1 of the Supporting Information). The analysis of the folding state hence relied on SEC, CD, and conductance measurements. LDAO appeared to be the most effective detergent in EMP's refolding. After refolding in LDAO

dx.doi.org/10.1021/bi500660q | Biochemistry 2014, 53, 4826−4838

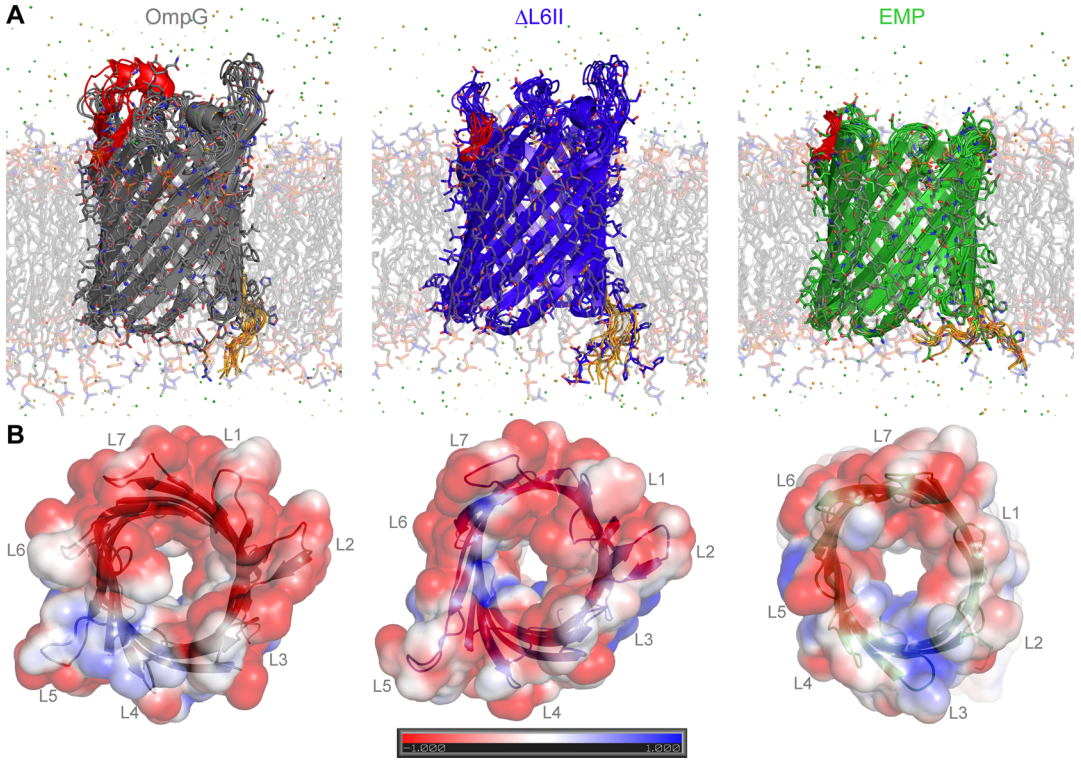

Figure 6. Molecular dynamics simulations of OmpG, ΔL6II, and EMP. (A) Mean conformation of the pores (4 ns each depicted structure) revealing the reduced height of the EMP relative to the lipid bilayer. (B) Electrostatics of the engineered extracellular part of the OmpG porin reveal a diminished overall charge of the EMP and a general decrease in negative charges.

micelles, the recombinant minimal porin eluted in size-exclusion chromatography like OmpG[58] mainly as a well-shaped peak corresponding to an apparent molecular mass of 85 kDa, and hence to the monomeric species of micelle-embedded EMP (Figure S7 of the Supporting Information; 26 kDa EMP and 59 kDa LDAO micelle). Interestingly, refolding attempts in other mild detergents such as OG, DM, and C_8E_4 failed to yield any homogeneous or monomeric EMP species. Western blotting and mass spectrometry confirmed the identity of the refolded monomers (Figure S7C of the Supporting Information).

CD analyses of the monomeric minimal porin indicated a β-barrel conformation, being highly comparable to those of OmpG and its L6 variants (Figure 2 and section S2 of the Supporting Information). Deconvolution of the 20 °C spectrum in DMPC revealed an increased relative β-sheet content, as expected after deletion of the extracellular loops (Table S1 of the Supporting Information). Thermal unfolding of EMP proceeded cooperatively and irreversibly, as shown by the strong hysteresis upon cooling as well as the hypsochromically shifted CD spectrum of heat-denatured porin. The reproducible CD spectra and the cooperative thermal unfolding confirmed the correct assembly of the minimal porin. Interestingly, the thermal stability of monomeric EMP was ~10 °C higher than that of its OmpG template, and hence in a range that prevented the exact determination of EMP's T_m (Figure S2 of the Supporting Information). Another difference with respect to OmpG is the stronger propensity of the monomeric minimal porin to aggregate at high temperatures. After thermal denaturation and cooling, the intensity of EMP's CD spectrum was reduced by ~60%. This reduction coincides with the observation of mild protein aggregation indicated by the increasing high-voltage/dynode signals of the spectrometer's photomultiplier during heating (particle-generated light scattering) (Figure S7D of the Supporting Information). Nevertheless, the engineered minimal porin is a highly robust protein as it can be stored for weeks at 4 °C without aggregation as judged by unaltered CD spectroscopic analyses.

OCD analyses of EMP in DMPC vesicles (Figure 2) revealed that the minimal porin responded by changing its orientation when it was present in bilayers below and above the lipid-phase transition temperature, as indicated by the 190 nm:218 nm signal ratio, while for OmpG and its L6 deletion variants, no changes had been observed. In the gel phase (20 °C), when the membrane is thicker because of the stretched conformation of its acyl constituents, the EMP's strong positive band (190 nm) indicated the expected tilted alignment previously observed for OmpG. At 35 °C, the significantly increased negative band (218 nm) indicated a more pronounced strand tilt, in response to the decreased thickness of the liquid phase of the bilayer. This suggests that correctly assembled EMP is sensitive to bilayer thickness and fluidity.

Electrophysiological Properties of EMP. BLM measurements showed for open channels of the engineered minimal porin conductances at least 1.2-fold higher (N = 38, and $P < 10^{-3}$) than those for open OmpG channels. The EMP conductances ranged from 0.86 ± 0.020 to 1.06 ± 0.036 nS and depended on the pH and chosen lipid bilayer (Figure 3). Observed gating behaviors were similar among different EMP preparations. Surprisingly, we observed partly closed states of EMP, although all structural elements, commonly suggested to be essential for OmpG gating, were removed. The partly closed states conducted at 26−66% of the open state. Furthermore, the occupancy and amplitude of these closed states depended

dx.doi.org/10.1021/bi500660q | Biochemistry 2014, 53, 4826−4838

on the type of lipid bilayer and pH value. In asolectin at pH 7.4, EMP channels acquired only two partly closed states with conductances of 0.64 ± 0.015 nS (S_1; N = 19) and 0.38 ± 0.014 nS (S_2; N = 9). Under acidic conditions (pH 5.0), an open state (for S_0, 0.92 ± 0.026 nS and N = 19) and two partly closed states (for S_1, 0.47 ± 0.020 nS and N = 23; for S_2, 0.24 ± 0.015 nS and N = 11) were identified. EMP showed similar conductances for its open, S_1, and S_2 states also in DPhPC bilayers. At neutral pH, the artificial minimal channel switched between the open (for S_0, 1.06 ± 0.036 nS and N = 21) and two partly closed states (for S_1, 0.67 ± 0.050 nS and N = 17; for S_2, 0.42 ± 0.050 nS and N = 8), while at pH 5.0, the conductance of all states was reduced to 0.86 ± 0.020 nS (S_0; N = 35), 0.52 ± 0.028 nS (S_1; N = 24), and 0.28 ± 0.016 nS (S_2; N = 30) (Figure 3).

The EMP channel differed from the OmpG templates also by its distinct gating characteristics, with open probabilities and transition frequencies being highly dependent on the bilayer properties (Figure 7). In asolectin membranes and at pH 7.4, global open probability P_o of EMP channels was reduced 6-fold, and gating event frequency f was reduced 5-fold compared to that of OmpG (Figure 7C). Accordingly, the 2D event distribution plots as derived from current recordings of EMP in asolectin membranes (80 mV) revealed few gating events with long durations in the range of 31 ms to 1 s (Figure 7). Reconstitution of the engineered minimal channels in DPhPC membranes had a weaker effect on the gating characteristics, with P_o and f being reduced by factors of only 2 and 3, respectively, relative to those of OmpG (Figure 7C). As with asolectin, the mean dwell times of EMP gating in DPhPC ranged from 1 ms to 31 s (Figure 7). Interestingly, under acidic conditions, the previous effects were inverted, and EMP channels displayed now stronger gating characteristics in asolectin than in DPhPC membranes.

DISCUSSION

Robustness of the OmpG Porin as a Protein Engineering Template. The structure of the ΔL6II variant of OmpG shows a largely unchanged β-barrel with differences mainly in the loop regions, in agreement with previous reports,[15,20,26] thus confirming the general tolerance of this β-barrel porin to reengineering. Differences are caused by a lack of stabilizing interactions with the L6 β-hairpin of ΔL6II as well as by the different crystal packing. In ΔL6II, the truncated L6 loop adopted a conformation more open than that in OmpG, explaining the similar conductance values obtained via BLM measurements (Figures 3 and 5). On the basis of the five different forms of OmpG crystal packings (Figure S4 of the Supporting Information), two essential hydrophobic interfaces were identified (Figure 5D,E). Although they are possibly crystallographic artifacts, they may explain the oligomerization tendencies of OmpG[59] and EMP. Accordingly, future engineering may address the modification of outer porin surfaces to foster selective oligomerization.

MD simulations showed robust and rigid barrels, though biochemical and electrophysiological behavior suggested dynamic structures, consistent with previous reports about OmpG[15] and VDAC.[60,61] Accordingly, the EMP design and its found characteristics may serve as a model system to resolve general issues of porins in terms of folding, gating behavior, and the role of structural and functional dynamics. We showed by a combination of various techniques like SEC, CD spectroscopy, and electrophysiological analyses that the engineered minimal

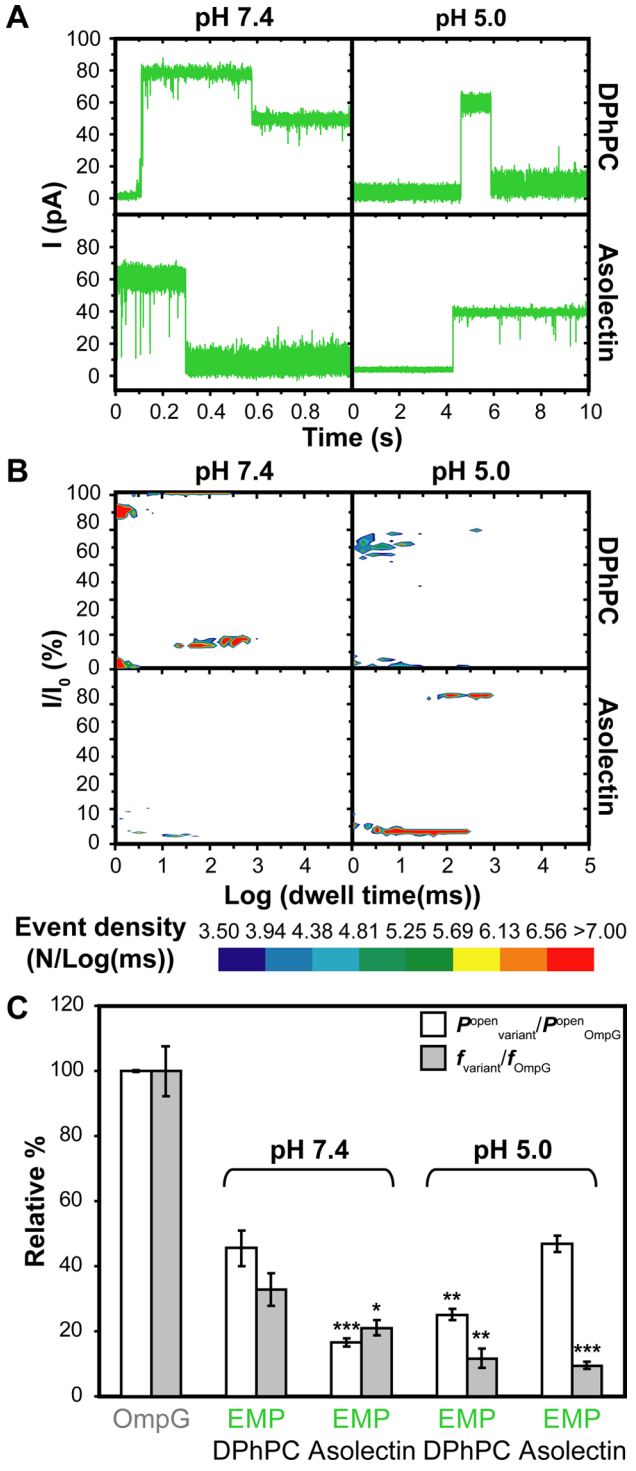

Figure 7. Influence of the pH and type of lipid on gating characteristics of EMP. (A) Typical 80 mV single-channel recordings of EMP at pH 7.4 or 5.0 in asolectin and DPhPC, used for the generation of the 2D distribution plots in panel B. (B) 2D event distribution plots of the switching behavior of EMP. The distribution of events for 30 s of recorded time is plotted according to current intensity I and dwell times. I (color code below the graphs) is expressed as a percentage of the highest intensity, I_o. (C) Comparison of the gating behavior of OmpG and EMP (Table S2 of the Supporting Information). f and P_o of EMP are expressed as a percentage of those of OmpG. Bars denote standard errors of triplicate measurements and asterisks statistically significant differences (paired t test; $^*P \geq 0.069$; $^{**}P < 0.0232$; $^{***}P \leq 0.0067$) with respect to values of EMP in DPhPC (pH 7.4).

dx.doi.org/10.1021/bi500660q | Biochemistry 2014, 53, 4826−4838

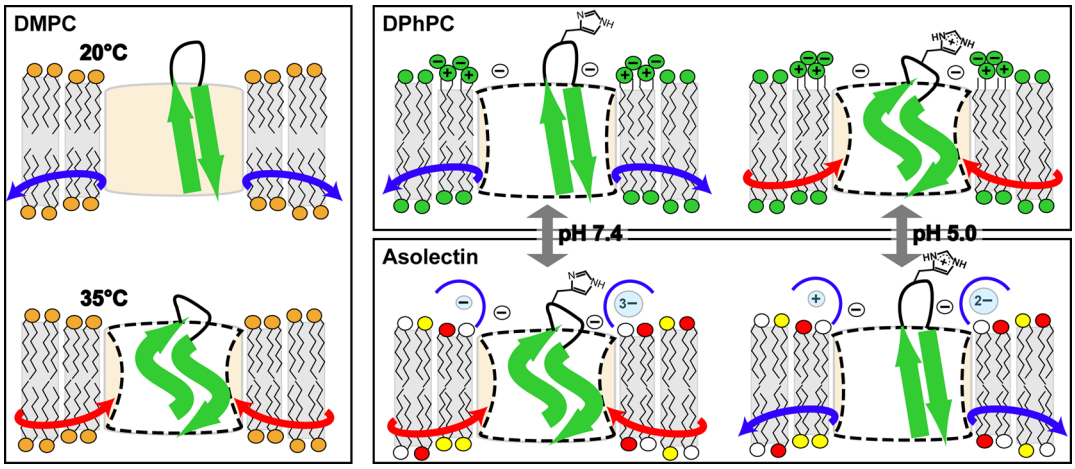

Figure 8. Hypothetical model on the elastic movements of the EMP barrel. In the gel phase of DMPC (20 °C), the height of the β-barrel matches the thickness of the bilayer. At 35 °C, where the liquid crystalline membrane is thinner, the pore becomes compressed (red arrow) and the β-strands acquire a more tilted alignment. In response to the membrane charge and fluidity, EMP shows inverted gating behavior in DPhPC and asolectin at pH 7.4 and 5.0.

porin forms a folded, well-behaving porin with features that strongly resemble in most aspects those of its OmpG template. First, we found a homogeneous EMP species by SEC that could be assigned to the predicted monomeric, micelle-embedded porin. Second, thermal unfolding showed cooperativity as required for a compact β-barrel architecture. Third, it forms a broad ion-conducting pore that shows a uniform conductance of 1.06 nS at neutral pH.

Shortening of Extracellular Loops Affects Membrane Insertion. Folding and reconstitution of the β-barrel in the presence of detergent micelles or lipid bilayers apparently take different routes. The direct insertion of denatured variants into preformed vesicles showed a preference of OmpG for DPPC, while the L6 variants with the shortened $\beta11-\beta12$ hairpin [compared to those of PDB entries 2IWW and 2IWV (Figure S5B of the Supporting Information)] preferred the shorter aliphatic chains of DMPC. In contrast, reconstitution of all detergent-refolded OmpG variants into DMPC vesicles or in planar bilayers of DPhPC or asolectin occurred with similar efficiencies (40−70%), even at temperatures below those of the lipid-phase transitions. These routes could potentially determine the direction of the inserted channel[62] or the type of assembly (monomer or dimer).[59] The shift in the preference for different lipids might be driven by (a) the reduction in barrel height and (b) the diminution of the surface charge (Figure 6).

For all variants, secondary structure analyses from CD data match those obtained from X-ray structures (Table S1 of the Supporting Information). Most interestingly, the OCD spectra of EMP in DMPC bilayers showed significant differences when the bilayer thickness changed upon transitions from the gel phase (20 °C) to the thinner liquid crystalline phase (35 °C), in contrast to the OmpG and L6 deletion variants. These changes can be interpreted in terms of an increased tilt angle of the β-strands in response to a compression by the bilayer. Having transformed the extracellular loops to short turns, EMP was converted to a more membrane-sensitive barrel responding to its lipidic environment. Additionally, elastic fluctuations in DMPC are stronger at 35 °C, and the levels of hydration of lipid headgroups[63] and protein increase (Table 1, blue shifts in OCD minima), thus allowing the barrel strands to acquire an orientation more parallel to the membrane plane. In response to the hydrophobic mismatch,[64] helical membrane proteins were shown to increase their tilt in lipid bilayers with shorter acyl chains[65] where elastic fluctuations of the lipid membrane are stronger.[16]

So far, OCD had been mostly applied to α-helical transmembrane elements such as the oncogenic E5 protein,[35] the platelet-derived growth factor receptor,[66] and channel-forming peptides.[41,67−70] Recently, a first example showing the orientation of a β-barrel structure to a membrane was presented.[71] This work provides thus further evidence that OCD can detect β-barrel tilts and in combination with biophysics enhances the understanding of membrane protein dynamics and domain mobility.

OmpG-like Porins Exhibit Loop-Independent Gating. Mobile regions of porins and channels are commonly considered to control gating activity; thus, elimination of these must generate a constitutively open pore. For OmpG, gradual shortening of L6 resulted in a sequential reduction of the level of spontaneous gating (Figure 4) and, together with the immobilization of L6 with an optimized H-bonding network,[15] provides first steps toward a putative sensor. However, closing events still occurred, albeit rarely, even though L6 could no longer fully occlude the pore. Surprisingly, loop-depleted EMP exhibits strong gating, though the only element still capable of closing the pore is the β-barrel itself. In mVDAC1, immobilization of the N-terminal helix altered the gating properties, events followed different routes, and complete closure occurred probably via semicollapsed β-barrel forms.[60] Interestingly, EMP responds to changes in bilayer thickness, as its β-strands realign relative to the membrane, probably reflecting barrel deformation. In contrast, in OmpG the interaction of L6 with the lipids has no overall effect on the pore structure.[27]

EMP channels were highly conducting with two subconducting states (Figure 3), exhibiting at least 3-fold fewer rapid transitions (f) than OmpG and the L6 deletion variants (Figure 4C) and with significantly reduced open probabilities (P_o). Current traces of the minimal porin appeared remarkably similar to current blockades resulting from modulators in αHL-like polyethylene glycols[72] or polypeptide loops.[12] Occupancy of these subconducting states cannot be solely attributed to the newly introduced β-turns, which are too short to protrude into

dx.doi.org/10.1021/bi500660q | Biochemistry 2014, 53, 4826−4838

the pore lumen and account for the blockages. Together with the susceptibility to the lipid bilayer, the subconducting states suggest that EMP gating depends on both lipid and pH (Figure 7). In the less compact and charged asolectin, at pH 7.4, the minimal porin showed a 16.5% P_o with an f 5-fold lower than that of OmpG. In zwitterionic DPhPC, EMP showed a 46% P_o and 3-fold lower f in comparison to those of OmpG. Under acidic conditions, this behavior was inverted, and the minimal pore appeared to have a higher P_o and a lower f. The corresponding Ohm plots yielded high- and low-conducting states at acidic pH in asolectin and DPhPC bilayers, respectively.

Although these changes may involve strand tilting, tilting on its own cannot account for this distinct gating. Reduction of the pore size of 19-stranded human VDAC1 by one and two strands[61] has produced 2- and 3.5-fold reductions in VDAC1's conductance, respectively. The smaller EMP exhibited an only 1.5−2-fold difference in conductance, depending on the pH and lipid composition. This change, albeit less significant than that observed in the larger VDAC1 porin, suggests that occlusion of the EMP pore by burial of its strands into the membrane is unlikely to cause the defined subconducting states observed in the current measurements. However, a semi-collapsed, ellipsoidal minimal porin may be sufficiently narrowed to diminish ion entry and be responsible for the closing events at 35 °C and pH 7.4 (Figure 8). Alternatively, an occlusion of the pore by dipping into the membrane due to the diminished surface charge may be envisioned as a cause of the defined subconducting states but is unlikely due to the implied large-scale motion of the EMP transmembrane domain. For DMPC bilayers, a network of water bridges and charge pairing links 98% of the headgroups;[73] reorganization of these interactions could enforce structural changes in the barrel, accounting for further reduction of the P_o at pH 5.0 (Figure 8). In asolectin (40% PC, 16% PE, 11% PI, and 33% polar charged lipids), the phase transition temperature is below the biologically relevant range. As a consequence, at 20 °C and pH 7.4, the effects on the barrel wall resemble those in DPhPC at 35 °C. Lowering the pH allows the barrel to acquire a more stretched conformation, because of a shift in the asolectin lipid-phase transition to higher temperatures or the formation of stabilizing electrostatic interactions that may involve H231 (Figure 8). The barrel movements responsible for the gating in EMP might be the origin of the residual gating observed for ΔL6II and the optimized OmpG variant reported by Chen et al.,[15] as well. Sadly, native OmpG evades these analyses by its habitual flickering caused by L6.

CONCLUSIONS

This work aimed to enhance OmpG's gating for advanced protein engineering. The shortening of L6 by 12 amino acids (ΔL6II) successfully reduced the spontaneous gating (f) of OmpG while leaving the open probability (P_o) of the channel unaffected, thus offering a useful template for advanced engineering. However, EMP's behavior was unexpected. Instead of providing a fully open channel, a pore exhibiting a 50% P_o with an f strongly affected by temperature and membrane compactness was obtained. Loop rearrangements in OmpG appear to control its spontaneous gating, but they are not the sole requirement for the channel's conducting ability. Residual gating, as observed in the L6 deletion variants, and the unique gating behavior of EMP most probably involve partial or global conformational changes of the β-barrel wall. This strengthens the view that porins form rather dynamic structures reversibly responding to the mechanical properties of the surrounding bilayer. Elastic barrel movements and acquisition of semi-collapsed/ellipsoidal conformations explain the observed loop-independent complete channel closure and allow a deeper understanding of the gating of other porins. These movements need to be considered in the design of more effective nanopores, as they can potentially regulate the flux of compounds across the membrane.

ASSOCIATED CONTENT

Supporting Information

Eight figures, two tables, supporting experimental procedures, and supporting results. This material is available free of charge via the Internet at http://pubs.acs.org.

Accession Codes

Coordinates and structure factors for the OmpG ΔL6II variant were deposited in the Protein Data Bank as entry 4CTD.

AUTHOR INFORMATION

Corresponding Author

*E-mail: essen@chemie.uni-marburg.de. Phone: +49 6421 28 22032.

Author Contributions

W.G. and G.P. contributed equally to this work.

Funding

We thank DFG (ES152/8) for financial support. W.G. has received funding from a Marie Curie Actions IEF of the EU's FP7 (2007−2013) under REA Grant n° 330915: SigT-OR-G and the ITN SBMP.

Notes

The authors declare no competing financial interest.

ACKNOWLEDGMENTS

We thank S.-L. Tsougaraki for line editing and the ESRF ID 14-1 and local contact T. Klar.

ABBREVIATIONS

αHL, α-hemolysin; asu, asymmetric symmetry unit; C_8E_4, n-octyl tetraoxyethylene; CD, circular dichroism; DM, n-decyl β-D-maltoside; DMPC, 1,2-dimyristoyl-*sn*-glycero-3-phosphocholine; DOPC, 1,2-dioleoyl-*sn*-glycero-3-phosphocholine; DPPC, 1,2-dipalmitoyl-*sn*-glycero-3-phosphocholine; DPhPC, 1,2-diphytanoyl-*sn*-glycero-3-phosphocholine; EMP, engineered minimal porin; ESRF, European Synchrotron Radiation Facility; FTIR, Fourier transform infrared; L6, loop 6; LDAO, lauryldimethylamine-*N*-oxide; MRE, mean residue ellipticity; OCD, oriented CD; OG, n-octyl β-D-glucopyranoside; OmpF, outer membrane protein F; OmpG, outer membrane protein G; P_o, open probability; rmsd, root-mean-square deviation; SEM, standard error of the mean; TLC, thin-layer chromatography; VDAC, voltage-dependent anion channel; 2D, two-dimensional.

REFERENCES

(1) Banghart, M. R., Volgraf, M., and Trauner, D. (2006) Engineering light-gated ion channels. *Biochemistry 45*, 15129−15141.

(2) Grosse, W., Essen, L. O., and Koert, U. (2011) Strategies and perspectives in ion-channel engineering. *ChemBioChem 12*, 830−839.

(3) Woodhouse, G., King, L., Wieczorek, L., Osman, P., and Cornell, B. (1999) The ion channel switch biosensor. *J. Mol. Recognit. 12*, 328−334.

(4) Hall, A. R., Scott, A., Rotem, D., Mehta, K. K., Bayley, H., and Dekker, C. (2010) Hybrid pore formation by directed insertion of α-haemolysin into solid-state nanopores. *Nat. Nanotechnol. 5*, 874−877.
(5) An, N., Fleming, A. M., White, H. S., and Burrows, C. J. (2012) Crown ether-electrolyte interactions permit nanopore detection of individual DNA abasic sites in single molecules. *Proc. Natl. Acad. Sci. U.S.A. 109*, 11504−11509.
(6) Mourot, A., Tochitsky, I., and Kramer, R. H. (2013) Light at the end of the channel: Optical manipulation of intrinsic neuronal excitability with chemical photoswitches. *Front. Mol. Neurosci. 6*, 5.
(7) Gradinaru, V., Mogri, M., Thompson, K. R., Henderson, J. M., and Deisseroth, K. (2009) Optical deconstruction of parkinsonian neural circuitry. *Science 324*, 354−359.
(8) Busskamp, V., and Roska, B. (2011) Optogenetic approaches to restoring visual function in retinitis pigmentosa. *Curr. Opin. Neurobiol. 21*, 942−946.
(9) Reitz, S., Cebi, M., Reiss, P., Studnik, G., Linne, U., Koert, U., and Essen, L. O. (2009) On the function and structure of synthetically modified porins. *Angew. Chem., Int. Ed. 48*, 4853−4857.
(10) Miedema, H., Meter-Arkema, A., Wierenga, J., Tang, J., Eisenberg, B., Nonner, W., Hektor, H., Gillespie, D., and Meijberg, W. (2004) Permeation properties of an engineered bacterial OmpF porin containing the EEEE-locus of Ca^{2+} channels. *Biophys. J. 87*, 3137−3147.
(11) Naveed, H., Jimenez-Morales, D., Tian, J., Pasupuleti, V., Kenney, L. J., and Liang, J. (2012) Engineered oligomerization state of OmpF protein through computational design decouples oligomer dissociation from unfolding. *J. Mol. Biol. 419*, 89−101.
(12) Jung, Y., Bayley, H., and Movileanu, L. (2006) Temperature-responsive protein pores. *J. Am. Chem. Soc. 128*, 15332−15340.
(13) Stoddart, D., Maglia, G., Mikhailova, E., Heron, A. J., and Bayley, H. (2010) Multiple base-recognition sites in a biological nanopore: Two heads are better than one. *Angew. Chem., Int. Ed. 49*, 556−559.
(14) Banerjee, A., Mikhailova, E., Cheley, S., Gu, L. Q., Montoya, M., Nagaoka, Y., Gouaux, E., and Bayley, H. (2010) Molecular bases of cyclodextrin adapter interactions with engineered protein nanopores. *Proc. Natl. Acad. Sci. U.S.A. 107*, 8165−8170.
(15) Chen, M., Khalid, S., Sansom, M. S., and Bayley, H. (2008) Outer membrane protein G: Engineering a quiet pore for biosensing. *Proc. Natl. Acad. Sci. U.S.A. 105*, 6272−6277.
(16) Marsh, D., Shanmugavadivu, B., and Kleinschmidt, J. H. (2006) Membrane elastic fluctuations and the insertion and tilt of β-barrel proteins. *Biophys. J. 91*, 227−232.
(17) Liang, B., and Tamm, L. K. (2007) Structure of outer membrane protein G by solution NMR spectroscopy. *Proc. Natl. Acad. Sci. U.S.A. 104*, 16140−16145.
(18) Subbarao, G. V., and van den Berg, B. (2006) Crystal structure of the monomeric porin OmpG. *J. Mol. Biol. 360*, 750−759.
(19) Yildiz, O., Vinothkumar, K. R., Goswami, P., and Kuhlbrandt, W. (2006) Structure of the monomeric outer-membrane porin OmpG in the open and closed conformation. *EMBO J. 25*, 3702−3713.
(20) Grosse, W., Reiss, P., Reitz, S., Cebi, M., Lubben, W., Koert, U., and Essen, L. O. (2010) Structural and functional characterization of a synthetically modified OmpG. *Bioorg. Med. Chem. 18*, 7716−7723.
(21) van der Hoeven, R., and Forst, S. (2009) OpnS, an Outer Membrane Porin of *Xenorhabdus nematophila*, Confers a Competitive Advantage for Growth in the Insect Host. *J. Bacteriol. 191*, 5471−5479.
(22) Eren, E., Vijayaraghavan, J., Liu, J. M., Cheneke, B. R., Touw, D. S., Lepore, B. W., Indic, M., Movileanu, L., and van den Berg, B. (2012) Substrate Specificity within a Family of Outer Membrane Carboxylate Channels. *PLoS Biol. 10*, e1001242.
(23) Bond, P. J., Derrick, J. P., and Sansom, M. S. (2007) Membrane simulations of OpcA: Gating in the loops? *Biophys. J. 92*, L23−L25.
(24) Maruvada, R., and Kim, K. S. (2011) Extracellular loops of the *Escherichia coli* outer membrane protein A contribute to the pathogenesis of meningitis. *J. Infect. Dis. 203*, 131−140.
(25) Conlan, S., Zhang, Y., Cheley, S., and Bayley, H. (2000) Biochemical and biophysical characterization of OmpG: A monomeric porin. *Biochemistry 39*, 11845−11854.
(26) Korkmaz-Ozkan, F., Koster, S., Kuhlbrandt, W., Mantele, W., and Yildiz, O. (2010) Correlation between the OmpG secondary structure and its pH-dependent alterations monitored by FTIR. *J. Mol. Biol. 401*, 56−67.
(27) Zhuang, T., Chisholm, C., Chen, M., and Tamm, L. K. (2013) NMR-based Conformational Ensembles Explain pH-Gated Opening and Closing of OmpG Channel. *J. Am. Chem. Soc. 135*, 15101−15113.
(28) Prilipov, A., Phale, P. S., Van Gelder, P., Rosenbusch, J. P., and Koebnik, R. (1998) Coupling site-directed mutagenesis with high-level expression: Large scale production of mutant porins from *E. coli*. *FEMS Microbiol. Lett. 163*, 65−72.
(29) Neves, P., Lopes, S. C., Sousa, I., Garcia, S., Eaton, P., and Gameiro, P. (2009) Characterization of membrane protein reconstitution in LUVs of different lipid composition by fluorescence anisotropy. *J. Pharm. Biomed. Anal. 49*, 276−281.
(30) Surrey, T., and Jahnig, F. (1992) Refolding and oriented insertion of a membrane protein into a lipid bilayer. *Proc. Natl. Acad. Sci. U.S.A. 89*, 7457−7461.
(31) Mertins, B., Psakis, G., Grosse, W., Back, K. C., Salisowski, A., Reiss, P., Koert, U., and Essen, L. O. (2012) Flexibility of the N-terminal mVDAC1 segment controls the channel's gating behavior. *PLoS One 7*, e47938.
(32) Eriks, L. R., Mayor, J. A., and Kaplan, R. S. (2003) A strategy for identification and quantification of detergents frequently used in the purification of membrane proteins. *Anal. Biochem. 323*, 234−241.
(33) Klammt, C., Schwarz, D., Dotsch, V., and Bernhard, F. (2007) Cell-free production of integral membrane proteins on a preparative scale. *Methods Mol. Biol. 375*, 57−78.
(34) Psakis, G., Saidijam, M., Shibayama, K., Polaczek, J., Bettaney, K. E., Baldwin, J. M., Baldwin, S. A., Hope, R., Essen, L. O., Essenberg, R. C., and Henderson, P. J. (2009) The sodium-dependent D-glucose transport protein of *Helicobacter pylori*. *Mol. Microbiol. 71*, 391−403.
(35) Windisch, D., Hoffmann, S., Afonin, S., Vollmer, S., Benamira, S., Langer, B., Burck, J., Muhle-Goll, C., and Ulrich, A. S. (2010) Structural role of the conserved cysteines in the dimerization of the viral transmembrane oncoprotein E5. *Biophys. J. 99*, 1764−1772.
(36) van Stokkum, I. H., Spoelder, H. J., Bloemendal, M., van Grondelle, R., and Groen, F. C. (1990) Estimation of protein secondary structure and error analysis from circular dichroism spectra. *Anal. Biochem. 191*, 110−118.
(37) Provencher, S. W., and Glockner, J. (1981) Estimation of globular protein secondary structure from circular dichroism. *Biochemistry 20*, 33−37.
(38) Whitmore, L., and Wallace, B. A. (2004) DICHROWEB, an online server for protein secondary structure analyses from circular dichroism spectroscopic data. *Nucleic Acids Res. 32*, W668−W673.
(39) Lobley, A., Whitmore, L., and Wallace, B. A. (2002) DICHROWEB: An interactive website for the analysis of protein secondary structure from circular dichroism spectra. *Bioinformatics 18*, 211−212.
(40) Sreerama, N., and Woody, R. W. (2000) Estimation of protein secondary structure from circular dichroism spectra: Comparison of CONTIN, SELCON, and CDSSTR methods with an expanded reference set. *Anal. Biochem. 287*, 252−260.
(41) Burck, J., Roth, S., Wadhwani, P., Afonin, S., Kanithasen, N., Strandberg, E., and Ulrich, A. S. (2008) Conformation and membrane orientation of amphiphilic helical peptides by oriented circular dichroism. *Biophys. J. 95*, 3872−3881.
(42) Kabsch, W. (2010) XDS. *Acta Crystallogr. D66*, 125−132.
(43) Terwilliger, T. C., Grosse-Kunstleve, R. W., Afonine, P. V., Moriarty, N. W., Zwart, P. H., Hung, L. W., Read, R. J., and Adams, P. D. (2008) Iterative model building, structure refinement and density modification with the PHENIX AutoBuild wizard. *Acta Crystallogr. D64*, 61−69.
(44) Emsley, P., and Cowtan, K. (2004) Coot: Model-building tools for molecular graphics. *Acta Crystallogr. D60*, 2126−2132.
(45) Chen, V. B., Arendall, W. B., III, Headd, J. J., Keedy, D. A., Immormino, R. M., Kapral, G. J., Murray, L. W., Richardson, J. S., and

Richardson, D. C. (2010) MolProbity: All-atom structure validation for macromolecular crystallography. *Acta Crystallogr. D66*, 12−21.
(46) Krissinel, E., and Henrick, K. (2007) Inference of macromolecular assemblies from crystalline state. *J. Mol. Biol. 372*, 774−797.
(47) Sali, A., and Blundell, T. L. (1993) Comparative protein modelling by satisfaction of spatial restraints. *J. Mol. Biol. 234*, 779−815.
(48) Kuntal, B. K., Aparoy, P., and Reddanna, P. (2010) EasyModeller: A graphical interface to MODELLER. *BMC Res. Notes 3*, 226.
(49) Anandakrishnan, R., Aguilar, B., and Onufriev, A. V. (2012) H+ + 3.0: Automating pK prediction and the preparation of biomolecular structures for atomistic molecular modeling and simulations. *Nucleic Acids Res. 40*, W537−W541.
(50) Bashford, D., and Karplus, M. (1990) pKa's of ionizable groups in proteins: Atomic detail from a continuum electrostatic model. *Biochemistry 29*, 10219−10225.
(51) Gordon, J. C., Myers, J. B., Folta, T., Shoja, V., Heath, L. S., and Onufriev, A. (2005) H++: A server for estimating pKas and adding missing hydrogens to macromolecules. *Nucleic Acids Res. 33*, W368−W371.
(52) Myers, J., Grothaus, G., Narayanan, S., and Onufriev, A. (2006) A simple clustering algorithm can be accurate enough for use in calculations of pKs in macromolecules. *Proteins 63*, 928−938.
(53) Jo, S., Kim, T., Iyer, V. G., and Im, W. (2008) CHARMM-GUI: A web-based graphical user interface for CHARMM. *J. Comput. Chem. 29*, 1859−1865.
(54) Woolf, T. B., and Roux, B. (1996) Structure, energetics, and dynamics of lipid-protein interactions: A molecular dynamics study of the gramicidin A channel in a DMPC bilayer. *Proteins 24*, 92−114.
(55) Phillips, J. C., Braun, R., Wang, W., Gumbart, J., Tajkhorshid, E., Villa, E., Chipot, C., Skeel, R. D., Kale, L., and Schulten, K. (2005) Scalable molecular dynamics with NAMD. *J. Comput. Chem. 26*, 1781−1802.
(56) Baker, N. A., Sept, D., Joseph, S., Holst, M. J., and McCammon, J. A. (2001) Electrostatics of nanosystems: Application to microtubules and the ribosome. *Proc. Natl. Acad. Sci. U.S.A. 98*, 10037−10041.
(57) Woody, R. W. (1993) The Circular-Dichroism of Oriented β Sheets: Theoretical Predictions. *Tetrahedron: Asymmetry 4*, 529−544.
(58) Conlan, S., and Bayley, H. (2003) Folding of a Monomeric Porin, OmpG, in Detergent Solution. *Biochemistry 42*, 9453−9465.
(59) Mari, S. A., Koster, S., Bippes, C. A., Yildiz, O., Kuhlbrandt, W., and Muller, D. J. (2010) pH-induced conformational change of the β-barrel-forming protein OmpG reconstituted into native *E. coli* lipids. *J. Mol. Biol. 396*, 610−616.
(60) Zachariae, U., Schneider, R., Briones, R., Gattin, Z., Demers, J. P., Giller, K., Maier, E., Zweckstetter, M., Griesinger, C., Becker, S., Benz, R., de Groot, B. L., and Lange, A. (2012) β-Barrel mobility underlies closure of the voltage-dependent anion channel. *Structure 20*, 1540−1549.
(61) Reina, S., Magri, A., Lolicato, M., Guarino, F., Impellizzeri, A., Maier, E., Benz, R., Ceccarelli, M., De Pinto, V., and Messina, A. (2013) Deletion of β-strands 9 and 10 converts VDAC1 voltage-dependence in an asymmetrical process. *Biochim. Biophys. Acta 1827*, 793−805.
(62) Chen, M., Li, Q. H., and Bayley, H. (2008) Orientation of the monomeric porin OmpG in planar lipid bilayers. *ChemBioChem 9*, 3029−3036.
(63) Trapp, M., Gutberlet, T., Juranyi, F., Unruh, T., Deme, B., Tehei, M., and Peters, J. (2010) Hydration dependent studies of highly aligned multilayer lipid membranes by neutron scattering. *J. Chem. Phys. 133*, 164505.
(64) Ramakrishnan, M., Qu, J., Pocanschi, C. L., Kleinschmidt, J. H., and Marsh, D. (2005) Orientation of β-barrel proteins OmpA and FhuA in lipid membranes. Chain length dependence from infrared dichroism. *Biochemistry 44*, 3515−3523.
(65) Anbazhagan, V., Qu, J., Kleinschmidt, J. H., and Marsh, D. (2008) Incorporation of outer membrane protein OmpG in lipid membranes: Protein-lipid interactions and β-barrel orientation. *Biochemistry 47*, 6189−6198.
(66) Muhle-Goll, C., Hoffmann, S., Afonin, S., Grage, S. L., Polyansky, A. A., Windisch, D., Zeitler, M., Burck, J., and Ulrich, A. S. (2012) Hydrophobic matching controls the tilt and stability of the dimeric platelet-derived growth factor receptor (PDGFR) β transmembrane segment. *J. Biol. Chem. 287*, 26178−26186.
(67) Vogel, H. (1987) Comparison of the conformation and orientation of alamethicin and melittin in lipid membranes. *Biochemistry 26*, 4562−4572.
(68) Qian, S., Wang, W., Yang, L., and Huang, H. W. (2008) Structure of transmembrane pore induced by Bax-derived peptide: Evidence for lipidic pores. *Proc. Natl. Acad. Sci. U.S.A. 105*, 17379−17383.
(69) Weiss, T. M., Yang, L., Ding, L., Waring, A. J., Lehrer, R. I., and Huang, H. W. (2002) Two states of cyclic antimicrobial peptide RTD-1 in lipid bilayers. *Biochemistry 41*, 10070−10076.
(70) Yang, L., Harroun, T. A., Weiss, T. M., Ding, L., and Huang, H. W. (2001) Barrel-stave model or toroidal model? A case study on melittin pores. *Biophys. J. 81*, 1475−1485.
(71) Ruskamo, S., Yadav, R. P., Sharma, S., Lehtimaki, M., Laulumaa, S., Aggarwal, S., Simons, M., Burck, J., Ulrich, A. S., Juffer, A. H., Kursula, I., and Kursula, P. (2014) Atomic resolution view into the structure-function relationships of the human myelin peripheral membrane protein P2. *Acta Crystallogr. D70*, 165−176.
(72) Movileanu, L., Cheley, S., and Bayley, H. (2003) Partitioning of individual flexible polymers into a nanoscopic protein pore. *Biophys. J. 85*, 897−910.
(73) Pasenkiewicz-Gierula, M., Takaoka, Y., Miyagawa, H., Kitamura, K., and Kusumi, A. (1999) Charge pairing of headgroups in phosphatidylcholine membranes: A molecular dynamics simulation study. *Biophys. J. 76*, 1228−1240.